First measurement of $\Gamma(D_s^+ \to \mu^+ \nu)/\Gamma(D_s^+ \to \phi\pi^+)$

D. Acosta,[1] M. Athanas,[1] G. Masek,[1] H. Paar,[1] A. Bean,[2] J. Gronberg,[2] R. Kutschke,[2] S. Menary,[2] R. J. Morrison,[2] S. Nakanishi,[2] H. N. Nelson,[2] T. K. Nelson,[2] J. D. Richman,[2] A. Ryd,[2] H. Tajima,[2] D. Schmidt,[2] D. Sperka,[2] M. S. Witherell,[2] M. Procario,[3] S. Yang,[3] R. Balest,[4] K. Cho,[4] M. Daoudi,[4] W. T. Ford,[4] D. R. Johnson,[4] K. Lingel,[4] M. Lohner,[4] P. Rankin,[4] J. G. Smith,[4] J. P. Alexander,[5] C. Bebek,[5] K. Berkelman,[5] D. Besson,[5] T. E. Browder,[5] D. G. Cassel,[5] H. A. Cho,[5] D. M. Coffman,[5] P. S. Drell,[5] R. Ehrlich,[5] R. S. Galik,[5] M. Garcia-Sciveres,[5] B. Geiser,[5] B. Gittelman,[5] S. W. Gray,[5] D. L. Hartill,[5] B. K. Heltsley,[5] C. D. Jones,[5] S. L. Jones,[5] J. Kandaswamy,[5] N. Katayama,[5] P. C. Kim,[5] D. L. Kreinick,[5] G. S. Ludwig,[5] J. Masui,[5] J. Mevissen,[5] N. B. Mistry,[5] C. R. Ng,[5] E. Nordberg,[5] M. Ogg,[5,*] J. R. Patterson,[5] D. Peterson,[5] D. Riley,[5] S. Salman,[5] M. Sapper,[5] H. Worden,[5] F. Würthwein,[5] P. Avery,[6] A. Freyberger,[6] J. Rodriguez,[6] R. Stephens,[6] J. Yelton,[6] D. Cinabro,[7] S. Henderson,[7] K. Kinoshita,[7] T. Liu,[7] M. Saulnier,[7] F. Shen,[7] R. Wilson,[7] H. Yamamoto,[7] B. Ong,[8] M. Selen,[8] A. J. Sadoff,[9] R. Ammar,[10] S. Ball,[10] P. Baringer,[10] D. Coppage,[10] N. Copty,[10] R. Davis,[10] N. Hancock,[10] M. Kelly,[10] N. Kwak,[10] H. Lam,[10] Y. Kubota,[11] M. Lattery,[11] J. K. Nelson,[11] S. Patton,[11] D. Perticone,[11] R. Poling,[11] V. Savinov,[11] S. Schrenk,[11] R. Wang,[11] M. S. Alam,[12] I. J. Kim,[12] B. Nemati,[12] J. J. O'Neill,[12] H. Severini,[12] C. R. Sun,[12] M. M. Zoeller,[12] G. Crawford,[13] C. M. Daubenmier,[13] R. Fulton,[13] D. Fujino,[13] K. K. Gan,[13] K. Honscheid,[13] H. Kagan,[13] R. Kass,[13] J. Lee,[13] R. Malchow,[13] F. Morrow,[13] Y. Skovpen,[13,†] M. Sung,[13] C. White,[13] J. Whitmore,[13] P. Wilson,[13] F. Butler,[14] X. Fu,[14] G. Kalbfleisch,[14] M. Lambrecht,[14] W. R. Ross,[14] P. Skubic,[14] J. Snow,[14] P. L. Wang,[14] M. Wood,[14] D. Bortoletto,[15] D. N. Brown,[15] J. Fast,[15] R. L. McIlwain,[15] T. Miao,[15] D. H. Miller,[15] M. Modesitt,[15] S. F. Schaffner,[15] E. I. Shibata,[15] I. P. J. Shipsey,[15] P. N. Wang,[15] M. Battle,[16] J. Ernst,[16] H. Kroha,[16] S. Roberts,[16] K. Sparks,[16] E. H. Thorndike,[16] C. H. Wang,[16] J. Dominick,[17] S. Sanghera,[17] V. Shelkov,[17] T. Skwarnicki,[17] R. Stroynowski,[17] I. Volobouev,[17] P. Zadorozhny,[17] M. Artuso,[18] D. He,[18] M. Goldberg,[18] N. Horwitz,[18] R. Kennett,[18] G. C. Moneti,[18] F. Muheim,[18] Y. Mukhin,[18] S. Playfer,[18] Y. Rozen,[18] S. Stone,[18] M. Thulasidas,[18] G. Vasseur,[18] G. Zhu,[18] J. Bartelt,[19] S. E. Csorna,[19] Z. Egyed,[19] V. Jain,[19] P. Sheldon,[19] D. S. Akerib,[20] B. Barish,[20] M. Chadha,[20] S. Chan,[20] D. F. Cowen,[20] G. Eigen,[20] J. S. Miller,[20] C. O'Grady,[20] J. Urheim,[20] and A. J. Weinstein[20]

(CLEO Collaboration)

[1]*University of California, San Diego, La Jolla, California 92093*
[2]*University of California, Santa Barbara, California 93106*
[3]*Carnegie-Mellon University, Pittsburgh, Pennsylvania 15213*
[4]*University of Colorado, Boulder, Colorado 80309-0390*
[5]*Cornell University, Ithaca, New York 14853*
[6]*University of Florida, Gainesville, Florida 32611*
[7]*Harvard University, Cambridge, Massachusetts 02138*
[8]*University of Illinois, Champaign-Urbana, Illinois 61801*
[9]*Ithaca College, Ithaca, New York 14850*
[10]*University of Kansas, Lawrence, Kansas 66045*
[11]*University of Minnesota, Minneapolis, Minnesota 55455*
[12]*State University of New York at Albany, Albany, New York 12222*
[13]*Ohio State University, Columbus, Ohio 43210*
[14]*University of Oklahoma, Norman, Oklahoma 73019*
[15]*Purdue University, West Lafayette, Indiana 47907*
[16]*University of Rochester, Rochester, New York 14627*
[17]*Southern Methodist University, Dallas, Texas 75275*
[18]*Syracuse University, Syracuse, New York 13244*
[19]*Vanderbilt University, Nashville, Tennessee 37235*
[20]*California Institute of Technology, Pasadena, California 91125*

(Received 3 August 1993)

We present a measurement of $\Gamma(D_s^+ \to \mu^+ \nu)/\Gamma(D_s^+ \to \phi\pi^+) = 0.245 \pm 0.052 \pm 0.074$. Using this ratio and $\mathcal{B}(D_s^+ \to \phi\pi^+) = (3.7 \pm 0.9)\%$ we extract $f_{D_s} = 344 \pm 37 \pm 52 \pm 42$ MeV, where the last error is due to the uncertainty in the $D_s^+ \to \phi\pi^+$ absolute branching ratio. This result is larger than most theoretical predictions.

PACS number(s): 13.20.Fc

*Permanent address: Carleton University, Ottawa, Canada K1S 5B6.
†Permanent address: INP, Novosibirsk, Russia.

I. INTRODUCTION

Purely leptonic decays of charged mesons are understood theoretically to occur via an annihilation of the two constituent quarks. The decay rate is sensitive to the wave-function overlap of the two quarks at zero spatial separation, which is parametrized as the meson decay constant. The decay rate at D_s^+ is given by the formula [1]

$$\Gamma(D_s^+ \to l^+ \nu) = \frac{1}{8\pi} G_F^2 f_{D_s}^2 m_l^2 M_{D_s} \left[1 - \frac{m_l^2}{M_{D_s}^2} \right]^2 |V_{cs}|^2 , \tag{1}$$

where f_{D_s} is the meson decay constant, M_{D_s} is the D_s mass, m_l is the mass of the final-state lepton, G_F is the Fermi coupling constant, and V_{cs} is the Cabibbo-Kobayashi-Maskawa (CKM) matrix element taken to have a value of 0.974 [2].

Meson decay constants play an important role in extracting interesting physics quantities from diverse measurements. For example, the measurement of the $B\bar{B}$ mixing ratio can be expressed as a function of the CKM parameters times f_B^2 [3]. At present it is difficult to measure purely leptonic B decays, so we must rely on theoretical calculations of f_B. It would be of great help to check these calculations against the measurement of other heavy quark decay constants such as f_D.

Predictions of the branching ratios for the three purely leptonic channels accessible to D_s^+ decay are provided by evaluating Eq. (1). The relative branching ratios are $10{:}1{:}2\times10^{-5}$ for τ^+, μ^+, and e^+, respectively. Unfortunately, the relatively copious $\tau^+\nu$ mode is difficult to search for because of the presence of at least two neutrinos in the final state.

In this paper we describe the detection of the decay $D_s^+ \to \mu^+ \nu$, or its charge conjugate. To aid in signal identification the D_s^+ candidates are required to be consistent with coming from a parent D_s^{*+} which decays to γD_s^+. To perform this measurement we directly detect the photon from the D_s^{*+} decay, and the muon from the D_s^+ decay, and indirectly detect the neutrino using missing momentum and energy.

Since charm fragmentation is known to produce relative high-momentum particles we require the D_s^{*+} candidates to have momenta above 2.4 GeV/c. The expected muon (or neutrino) and photon momentum distributions are shown in Fig. 1. After describing the selection of the muon and the photon, we will discuss our technique for detecting the neutrino using a missing momentum measurement. To evaluate the effectiveness of our method we use two samples of events from the data to simulate the process we are looking for. These are $D^{*0} \to \gamma D^0$ and $D^{*+} \to \pi^+ D^0$ where, in both cases, $D^0 \to K^- \pi^+$. The signals for these samples can be found in a previous publication [4]. These decays are used to simulate $D_s^+ \to \mu^+ \nu$ by eliminating the tracking chamber and calorimeter measurements of the π^+ and using the K^- as the muon.

There are many physics backgrounds that can imitate the process we are seeking. For real leptons the background levels are almost identical in electron final states and muon final states. For the purely leptonic decay we are considering, the electronic branching ratio is negligible in comparison with the muonic branching ratio. Pion and kaon decays also produce many more muons than electrons, but these are considered as part of the hadron to lepton fake rate, and are dealt with separately. The only physics processes that can contribute significantly more muons than electrons for lepton momenta above 2 GeV/c are $D_s^+ \to \mu^+ \nu$ and $D^+ \to \mu^+ \nu$. The latter is suppressed by the CKM angle [see Eq. (1)], and by an additional factor, due to the requirement that there be a parent $D^{*+} \to \gamma D^+$ transition, the branching ratio for which is only about 1% [4]. Thus, performing the identical analysis, except for selecting electrons rather than muons, will give us a quantitative background measurement. When comparing the muon and electron data corrections are made for the known differences in lepton detection efficiencies, fake rates, phase space, and bremsstrahlung.

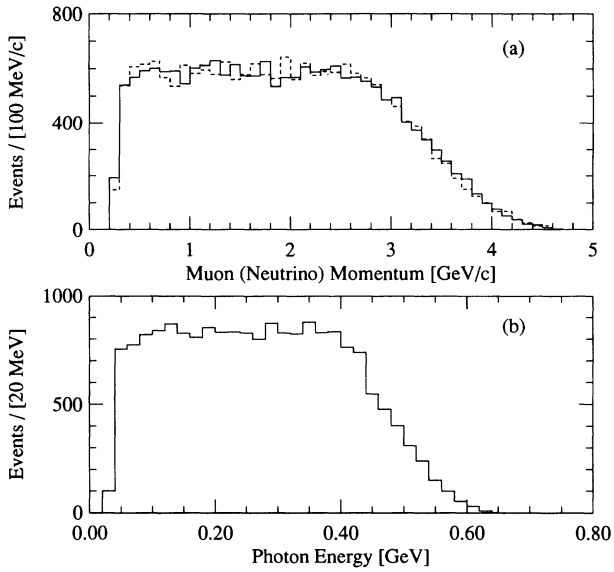

FIG. 1. The (a) muon (or neutrino), and (b) photon momentum distributions for $D_s^{*+} \to \gamma D_s^+$, $D_s^+ \to \mu^+ \nu$ decays, where D_s^{*+} is required to have momentum above 2.4 GeV/c.

The data sample used was collected with the CLEO II detector at the Cornell Electron Storage Ring (CESR). The integrated luminosity is 2.13 fb^{-1} collected at the $\Upsilon(4S)$ resonance or at energies just below. The CLEO II detector [5] is designed to detect both charged and neutral particles with excellent resolution and efficiency. The detector consists of a charged particle tracking system with three concentric drift chambers containing a total of 67 layers surrounded by a time-of-flight scintillation system and an electromagnetic shower detector consisting of 7800 thallium-doped cesium iodide crystals. The tracking system, time-of-flight scintillators, and calorimeter are installed inside a 1.5-T superconducting solenoidal magnet. Outside the magnet are iron and chambers for muon detection. The momentum resolution of the track-

ing system is given by $(\delta p/p)^2=(0.0015p)^2+(0.005)^2$, where p is in GeV/c. Ionization energy-loss information (dE/dx) is also measured in the main drift chamber. In the "good barrel" region, defined as the region where the angle θ of the shower with respect to the beam axis lies between 45° and 135°, the energy resolution for photons is given by

$$\delta E/E(\%)=0.35/E^{0.75}+1.9-0.1E$$

(E in GeV).

II. EVENT, LEPTON, AND PHOTON SELECTION

A. Event selection

A sample of relatively pure hadronic events is selected by imposing requirements that there be at least three good drift chamber tracks, that the total energy in tracks and showers be greater than 15% of the total center-of-mass energy $E_{\text{c.m.}}$ and that the total energy in the calorimeter be greater than 15% and less than 90% of $E_{\text{c.m.}}$. In addition the reconstructed event vertex must be consistent with the nominal interaction point. Additional criteria are used to eliminate low multiplicity sources of leptons such as QED processes and $\tau^+\tau^-$ pairs. We require that either the event has at least five well-reconstructed charged tracks, or at least three charged tracks accompanied by at least six neutral energy clusters. To suppress background caused by particles which escape detection at large $\cos\theta$, we require that the angle between the missing momentum of the event and the beam axis, $\theta_{p_{\text{miss}}}$, does not point along the beam direction, $|\cos\theta_{p_{\text{miss}}}|<0.9$.

B. Lepton identification and efficiencies

Since the electron sample is used to measure the background in the muon sample, the electron and muon analyses are performed with identical criteria, except for lepton identification. Both muons and electrons are selected with a minimum momentum of 2.4 GeV/c. This removes most of the leptons from B meson decays and is 33% efficient for $D_s^+\to\mu^+\nu$ [Fig. 1(a)].

To identify muons we require that track candidates penetrate at least seven interaction lengths of iron, and have $|\cos\theta|<0.85$. Tight track quality cuts are demanded to reduce the contamination from kaon and pion decays in flight. Once a track is found, the muon identification efficiency, measured with radiative muon pair events ($e^+e^-\to\mu^+\mu^-\gamma$), is (85±2)% in the momentum range of interest.

Electrons are selected on the basis of energy and shower shape measurements from the electromagnetic calorimeter, and momentum and dE/dx measurements from the tracking chambers. Electron candidates must pass the same solid angle and track quality requirements as muons. There is an additional source of electrons from photon conversions, 75% of which can be identified and rejected with a 1% loss of primary electrons. The overall electron identification efficiency is found by embedding tracks from radiative Bhabha events ($e^+e^-\to e^+e^-\gamma$) into hadronic events. This efficiency depends significantly on $\cos\theta$ outside the barrel region. We have found by analysis of generic continuum Monte Carlo data that the angular distribution of the lepton is $1+0.8\cos^2\theta$, leading to an overall electron identification efficiency of (87±4)%.

C. Photon selection

Photons must be in the "good barrel" region, $|\cos\theta|<0.71$. They must be isolated by more than 20° from any charged track, and have a shower shape for which the probability that the energy deposition is due to a single photon is greater than 99%. We require a minimum energy of 150 MeV to eliminate backgrounds caused by the large number of low-energy photons. This cut leaves 78% of the spectrum from D_s^{*+} decay untouched, as can be seen in Fig. 1(b).

Most detected photons are the result of π^0 decay. To reduce this source of background we calculate the invariant mass of our photon candidate with all other photons in the event that have more than 50 MeV of energy. Photon combinations which have invariant masses within two standard deviations ($\sigma\sim5$ MeV) of the π^0 mass are eliminated. This procedure rejects 40% of the random photon background with only a 13% loss of efficiency.

III. SIGNAL SHAPE AND EFFICIENCY

A. D meson reconstruction using missing momentum and energy

To reconstruct the decay $D_s^+\to\mu^+\nu$ we detect the neutrino using missing momentum and energy. We study these variables using our $D^{*+}\to\pi^+D^0$, $D^0\to K^-\pi^+$ sample, since this provides us with high statistics and negligible background. We select $K^-\pi^+$ combinations within ±20 MeV of the D^0 mass and require that the measured $D^{*+}-D^0$ mass difference be within ±2 MeV of the known mass difference [2]. After requiring the kaon to have a momentum above 2.4 GeV/c to simulate the lepton analysis there are 1844 events with a D^{*+} momentum above 2.4 GeV/c.

To use this sample, the measurements of the fast π^+ are removed from both the tracking chambers and the calorimeter, K^- is "identified" as a muon, and the slow π^+ is ignored. For the remaining charged tracks in the event we use the measured momentum and the energy based on the pion mass hypothesis unless there is a positive kaon or proton identification based on combined dE/dx and time-of-flight information [6]. We find it useful to divide the event into two hemispheres found by bisecting the thrust axis of the event, calculated from all well-reconstructed tracks and isolated showers in the calorimeter that have more than 30 MeV of energy.

The missing momentum $\mathbf{p}_{\text{miss}}$ and energy E_{miss} are calculated using only energy and momentum measurements $(E_i,\mathbf{p}_i)$ of charged tracks and showers in the hemisphere which contains the lepton (kaon) candidate. The missing energy is found according to

$$E_{\text{miss}}=E_{\text{beam}}-\sum E_i\ , \tag{2}$$

where E_{beam} is the energy of the CESR beam. The missing momentum is defined as

$$\mathbf{p}_{\text{miss}} = \mathbf{p}_{\text{thrust}} - \sum \mathbf{p}_i \ , \tag{3}$$

where the direction of p_{thrust} is given by the thrust axis of the whole event. The magnitude of p_{thrust} is given by

$$p^2_{\text{thrust}} = E^2_{\text{beam}} - m^2_{\text{jet}} \ , \tag{4}$$

where m_{jet} is the average mass of a charm quark jet. The value of m_{jet} is measured to be 3.2 GeV using our sample of fully reconstructed D^{*+} mesons.

The D meson invariant mass $M(\mu\nu)$ is calculated using the lepton (kaon) four-momentum and the missing four-momentum. The missing four-momentum is defined using $\mathbf{p}_{\text{miss}}$, and setting the fourth component equal to the magnitude of p_{miss}, i.e., assuming that the missing mass is zero. The result of this determination of missing momentum, using only one hemisphere, is shown in Fig. 2(a) where we plot $M(\mu\nu)$ versus the lepton momentum for the D^{*+} data sample. $M(\mu\nu)$ tends to peak lower than the D mass, especially for the larger lepton (kaon) momenta we are interested in. This distortion results from using the lepton (kaon), but not the neutrino (removed pion), to calculate the thrust axis of the event. We have used the D^{*+} data sample and a $D_s^+ \to \mu^+ \nu$ Monte Carlo sample to develop an empirical correction factor which is a function of both the lepton momentum and the angle between the lepton and the thrust axis. This correction moves the thrust axis of the event away from the lepton momentum to account for the unbalanced momentum perpendicular to the thrust axis. The shift is largest for small lepton momenta which correspond to large neutrino momenta [7].

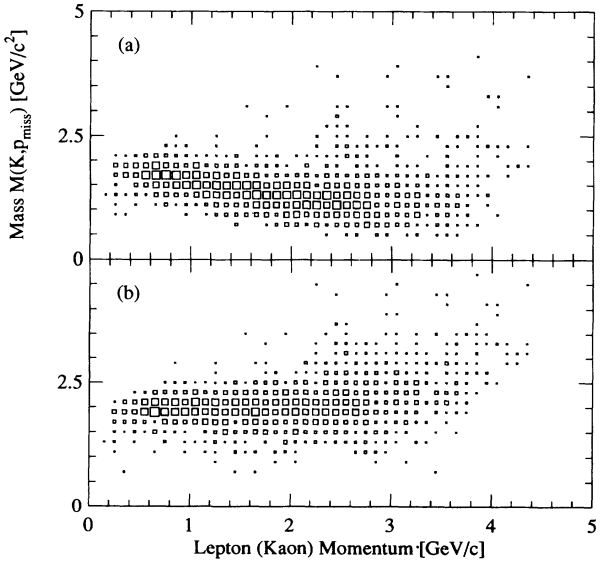

FIG. 2. Mass distribution of the lepton (kaon) and the missing momentum vector for the $D^{*+} \to \pi^+ D^0$, $D^0 \to K^- \pi^+$ event sample as a function of the lepton momentum for (a) the missing momentum defined by only the lepton hemisphere, and (b) with the empirical correction described in the text applied to (a).

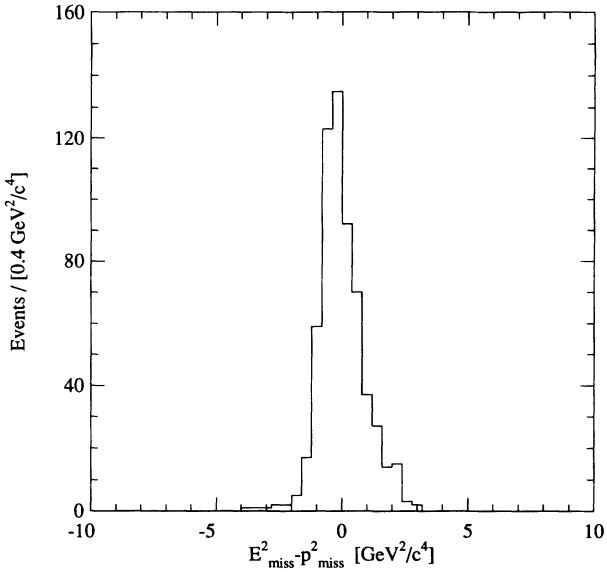

FIG. 3. Missing mass squared distribution for the $D^{*+} \to \pi^+ D^0$, $D^0 \to K^- \pi^+$ event sample for the missing momentum defined by only the lepton hemisphere with the empirical correction applied.

The result of determining the missing momentum after the empirical correction to the thrust axis is shown in Fig. 2(b). The value of $M(\mu\nu)$ for the D^{*+} sample is now independent of the lepton momentum. That this procedure works well is also shown by the distribution in missing mass squared for the D^{*+} data sample (Fig. 3). The missing mass squared, computed by subtracting p^2_{miss} from E^2_{miss}, has a distribution that peaks at zero and has a width of $\sigma = 0.75$ GeV^2 [8]. This agrees with the distribution expected from Monte Carlo studies.

B. $D^* - D$ mass difference

A D_s^+ candidate is selected by requiring $1.6 \text{ GeV} < M(\mu\nu) < 2.6$ GeV. The D_s^+ candidate is combined with a photon, selected as described above, and the mass difference ΔM is calculated as

$$\Delta M = M(\gamma\mu\nu) - M(\mu\nu) \ . \tag{5}$$

To understand what the ΔM distribution should look like, a data sample of $D^{*0} \to \gamma D^0$, $D^0 \to K^- \pi^+$ events is used. We select $K^- \pi^+$ combinations within ± 20 MeV of the D^0 mass, and again require that the kaon has a momentum greater than 2.4 GeV/c to simulate the lepton analysis. There is a substantial signal in the fully reconstructed mass difference $\delta M = M(\gamma K\pi) - M(K\pi)$ distribution but also significant background, so a δM sideband subtraction is always performed when using this data sample. Our sample contains 708 D^{*0} signal events with momenta larger than 2.4 GeV/c within ± 10 MeV of the known mass difference [9].

As with the D^{*+} sample we call the K^- a muon, eliminate the π^+, and perform the missing momentum analysis. After applying some additional background suppression cuts, described in Sec. V A, and subtracting

the δM sidebands, we obtain the mass difference distribution $\Delta M = M(\gamma K p_{\rm miss}) - M(K p_{\rm miss})$ shown in Fig. 4(a). There is a clear signal peak associated with the photon which can be parametrized as an asymmetric Gaussian with low side and high side σ's of 18 and 27 MeV, respectively, as compared to 5 MeV in the fully reconstructed sample. The shape of this distribution has been reproduced using $D^{*0} \to \gamma D^0$, $D^0 \to K^- \pi^+$ and $D_s^{*+} \to \gamma D_s^+$, $D_s^+ \to \mu^+ \nu$ Monto Carlo samples (Fig. 5). There is also a small flat component which results from replacing the correct photon with another photon.

The efficiency with respect to the fully reconstructed sample for an event to appear in the peak is $\epsilon_\nu = (25 \pm 3)\%$. The overall detection efficiency ϵ for the D_s^{*+} analysis is given by

$$\epsilon = \epsilon_\mu \epsilon_\gamma \epsilon_\nu \,, \tag{6}$$

where $\epsilon_\mu = (20 \pm 1)\%$ is the efficiency for having an identified muon above 2.4 GeV/c determined from the measured muon detection efficiency in $\mu^+\mu^-\gamma$ events, and the expected muon momentum spectrum in $D_s^+ \to \mu^+ \nu$ decays [Fig. 1(a)]. The efficiency for finding the correct photon from the D_s^{*+} is $\epsilon_\gamma = (48 \pm 2)\%$. This efficiency is obtained from Monte Carlo studies. The overall detection efficiency for $D_s^{*+} \to D_s^+ \gamma$, $D_s^+ \to \mu^+ \nu$ is $\epsilon = (2.4 \pm 0.3)\%$.

There are three additional contributions to the ΔM distribution which need to be considered. First there are direct $D_s^+ \to \mu^+ \nu$ decays which pair with a random photon to form a D_s^{*+} candidate. Second there are D_s^{*+} events where the correct photon is replaced by another photon. Third there is a small contribution from

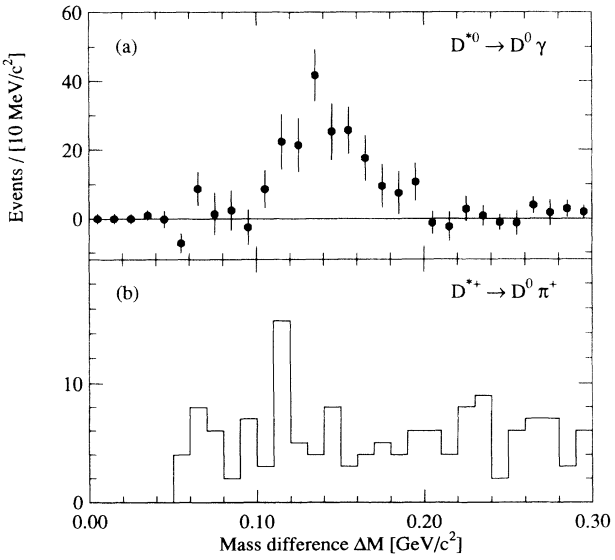

FIG. 4. The mass difference distributions for (a) the $D^{*0} \to \gamma D^0$, $D^0 \to K^- \pi^+$ event sample, eliminating the π^+ and using the missing momentum analysis described in the text. (b) The $D^{*+} \to \pi^+ D^0$, $D^0 \to K^- \pi^+$ event sample using the missing momentum analysis and combining with random photons.

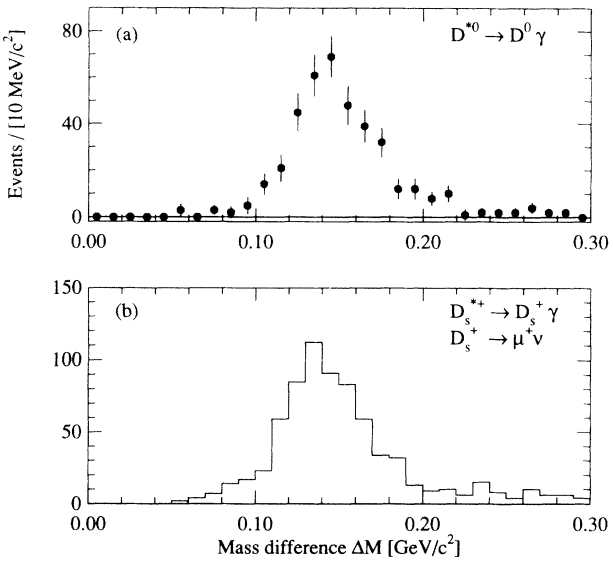

FIG. 5. The mass difference distributions from Monte Carlo data (a) for the $D^{*0} \to \gamma D^0$ sample where the D^0 is analyzed as $\mu^+ \nu$, and (b) for $D_s^{*+} \to \gamma D_s^+$, $D_s^+ \to \mu^+ \nu$.

$D^+ \to \mu^+ \nu$ decays combined with a random photon [4]. These contributions are simulated using the $D^{*+} \to \pi^+ D^0$ event sample, by combining the $M(K p_{\rm miss})$ candidates with random photons in the same event. In Fig. 4(b) we show the ΔM distribution from this sample.

The sum of all these contributions can be written as

$$N = \epsilon_\gamma N_{D_s^{*+}} + \epsilon_\gamma \epsilon_{\gamma'} N_{D_s^{*+}} + (1 - \epsilon_\gamma) \epsilon_{\gamma'} N_{D_s^{*+}} + \epsilon_{\gamma'} N_{D_s^+} + \epsilon_{\gamma'} N_{D^+} \,, \tag{7}$$

where $\epsilon_{\gamma'} = (31 \pm 5)\%$ is the efficiency for finding a random photon such that the event appears in the ΔM plot;

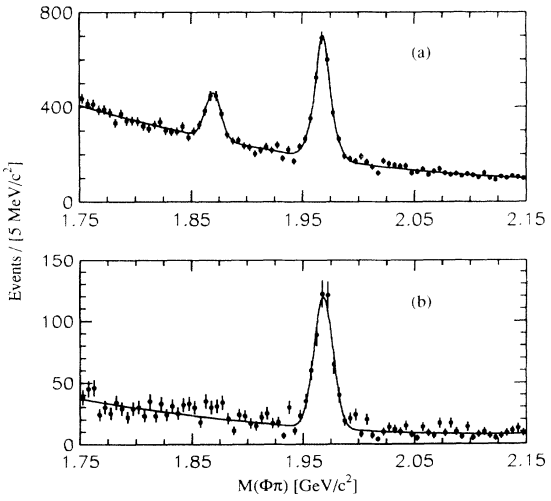

FIG. 6. The $\phi\pi^+$ mass distributions for (a) $\phi\pi^+$ and (b) $\gamma\phi\pi^+$ for candidate momenta above 2.4 GeV/c.

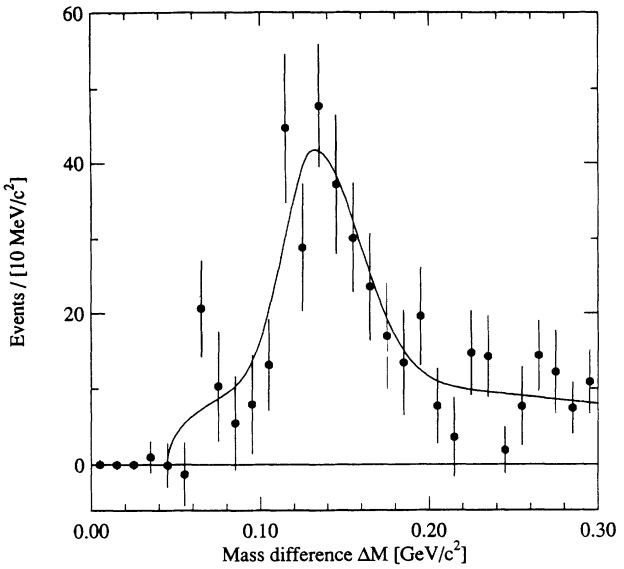

FIG. 7. The mass difference distribution expected for direct $D_s^{*+} \to \gamma D_s^+$, $D_s^+ \to \mu^+\nu$ decays summed with the random photon contribution from $D_s^+ \to \mu^+\nu$ and $D^+ \to \mu^+\nu$ decays. The distribution is the weighted sum of Figs. 4(a) and 4(b).

$N_{D_s^{*+}}$, $N_{D_s^+}$, and N_{D^+} are the number of muonic decays of the corresponding mesons. The first two terms are simulated by the D^{*0} sample, and the last three terms by the D^{*+} sample. From fully reconstructed $D_s^+ \to \phi\pi^+$ decays we measure the relative production ratio of D_s^{*+} to D_s^+ with D_s^{*+} momentum greater than 2.4 GeV/c to be 1.03 ± 0.20. The $\phi\pi^+$ mass distributions for D_s^{*+} and D_s^+ candidates are shown in Fig. 6. We also account for the small contribution from $D^+ \to \mu^+\nu$ decays [4]. The distributions in Figs. 4(a) and 4(b) are summed using appropriate weights to produce an expected signal distribution shown in Fig. 7. Overlaid is the result of a fit to a function which is the sum of the asymmetric Gaussian associated with the decay chain $D_s^{*+} \to \gamma D_s^+$, $D_s^+ \to \mu^+\nu$ and a $\sqrt{x - x_0}\, e^{-a(x-x_0)}$ piece which is used to describe the random photon component.

Since we are using radiative D^{*0} decays to simulate radiative D_s^{*+} decays, we must consider the presence of an extra $\bar{s}$ quark in the D_s^{*+} jet fragmentation. This could distort the mass difference distributions and the efficiencies, e.g., by producing an additional K_L in the same hemisphere, which would tend to lower the efficiency. As input to our Monte Carlo studies we have used fragmentation functions consistent with the experimental data for D_s^* and D^* mesons [10]. In Fig. 5, we show the mass difference distributions for Monte Carlo generated $D^{*0} \to \gamma D^0$, $D^0 \to K^-\pi^+$ and $D_s^{*+} \to D_s^+\gamma$, $D_s^+ \to \mu^+\nu$ decays. There is good agreement between them, and also between the D^{*0} Monte Carlo data, Fig. 5(a), and the D^{*0} data distribution in Fig. 4(a). The efficiency for an event to appear in the peak in Fig. 5 is $(2.4 \pm 0.1)\%$ for the D^{*0} Monte Carlo data, and $(2.8 \pm 0.1)\%$ for the D_s^{*+} Monte Carlo data, as compared with $(2.4 \pm 0.3)\%$ for the D^{*0} data. This is consistent with our expectation that D_s^{*+} jets are not very different from D^{*0} jets.

IV. BACKGROUND PROCESSES

A. Relative muon/electron ratio normalization

Most backgrounds have similar muon and electron ΔM distributions whereas $D_s^+ \to e^+\nu$ is negligible compared to $D_s^+ \to \mu^+\nu$. In order to subtract the electron data from the muon data we need to have a relatively precise measure of the muon/electron ratio normalization. Besides the relative efficiency numbers quoted above, corrections are made for differences in electron and muon radiation in the detector material (outer bremsstrahlung), the different probabilities that a photon is emitted in the decay (inner bremsstrahlung), and the differences in muon and electron phase space.

We have analyzed generic continuum Monte Carlo samples with $D_s^+ \to \mu^+\nu$ decays excluded to determine the most important contributions to the electron and muon backgrounds in the ΔM plot. The Monte Carlo simulation reproduces both the magnitude and the shape of the electron background well, but does not reproduce either the magnitude or the shape of the muon data unless a $D_s^+ \to \mu^+\nu$ contribution is included. The most important contributions to the background are the decay modes $D \to Kl\nu$ and $D_s \to \eta l\nu$, which comprise $\sim 75\%$ of the background. The decay mode $D \to \pi l\nu$ gives an additional $\sim 15\%$, while $\sim 5\%$ comes from $D \to K^* l\nu$ and $D_s \to \phi l\nu$. The contribution from $D_s \to \tau\nu$ with a leptonic τ decay is 5%. Given that there are large uncertainties in our current knowledge of charm semileptonic branching fractions [2], we regard this Monte Carlo study as a prudent check of our understanding of the backgrounds in our measurement, rather than a precise simulation of these backgrounds.

As a specific example of the near equality of the electron and muon rates we have made a detailed study of the decay mode $D^+ \to K^0 l\nu$, including radiative corrections (inner bremsstrahlung) according to the prescription of Atwood and Marciano [11], and the rate difference between muon and electron final states due to the lighter electron mass. For lepton momenta above 2.4 GeV/c the radiative corrections reduce the yields of electrons by 3.5% and of muons by 0.8%. This is counterbalanced by a 1.7% difference between muon and electron phase space, to give a muon/electron ratio excess of 1% for momenta above 2.4 GeV/c. The last correction is due to outer bremsstrahlung. This reduces the electron contribution relative to the muon contribution by 5%. Overall, taking into account that the electron detection efficiency is 2% higher than the muon efficiency we expect the muon sample from $D^+ \to K^0 l\nu$ to exceed the electron sample by 4%. For the other decay modes which contribute to both muon and electron samples we find small differences, which when averaged together also give a 4% excess of muons. Therefore, we use a correction factor of 1.04 ± 0.05 to multiply the electron sample.

B. Lepton fakes

It is necessary to determine the distribution in ΔM for both muon and electron fakes. This is accomplished by

using as leptons all charged tracks which satisfy our cuts. Identified leptons are subtracted out. We then multiply the measured ΔM distribution by the known fake rates for muon and electron identification [12]. The distribution of hadronic tracks entering the ΔM distribution is determined to be 60% pions, 27% kaons, and 13% protons from a continuum Monte Carlo study. Averaging over these species we find effective rates of $(0.61\pm0.14)\%$ for tracks faking muons and $(0.30\pm0.07)\%$ for tracks faking electrons, where we have included in the error a contribution from varying the kaon fraction between 17 and 37 %.

The fake distribution includes all possible contributions from hadronic D decays, the most serious of which are two-body decays. These contributions are suppressed by the fake rate, and by the detection of the second decay particle. The worst case is $D_s^{*+}\to\gamma D_s^+$, $D_s^+\to K^+K_L$, where the K^+ fakes a muon, and K_L is not detected. This contributes 0.8 events to the fake ΔM distribution.

V. RESULTS

A. Final analysis

After finding a lepton and a photon candidate we calculate the thrust axis of the event, and find the missing momentum, $p_{\rm miss}$, and energy, $E_{\rm miss}$, in the same hemisphere as the lepton, using Eqs. (2)–(4). The requirement $p_{\rm miss}>0.9$ GeV/c removes most of the fake lepton background. The expected neutrino momentum distribution for signal is shown in Fig. 1(a). We also require the missing mass squared to be consistent with a neutrino, $|E^2_{\rm miss}-p^2_{\rm miss}|<2$ GeV^2 (see Fig. 3).

The invariant mass of the lepton and missing momentum $M(\mu\nu)$ must be consistent with a D_s^+ meson, $1.6<M(\mu\nu)<2.6$ GeV, after making the empirical correction as a function of lepton momentum and angle of the lepton with respect to the thrust axis described above.

The D_s^{*+} candidate is constructed from the lepton, the photon, and the missing momentum [see Eq. (5)]. The D_s^{*+} candidate momentum must be larger than 2.4 GeV/c. We also insist that in the rest frame of the D_s^{*+} candidate, the cosine of the angle between the photon and the D_s^{*+} direction in the laboratory be larger than -0.7.

We are somewhat concerned with a small residual $b\to u l\nu$ background, since radiative corrections near the end point of the lepton spectrum affect the relative muon/electron ratio normalization. These events are more spherical than signal events, and can be suppressed by insisting that the thrust axis lines up with the D_s^{*+} candidate momentum such that the cosine of the angle between them is greater than 0.975. In Fig. 8, we show this distribution for our signal sample constructed from D^{*0} and D^{*+} events, compared with a Monte Carlo sample of $b\to u\mu\nu$ events surviving all the above cuts. The cut removes $\sim$70% of the residual $b\to u\mu\nu$ background leaving $\sim$10 muons from this source. The electron subtraction of this source is not exact due to radiative corrections, but would only leave a muon excess of $\sim$1 event.

B. Branching fraction

The resulting ΔM distributions for the muon and electron data are given in Fig. 9. Also shown is the calculation of the excess of muon fakes over electron fakes. The curve shows a likelihood fit to the muon spectrum from

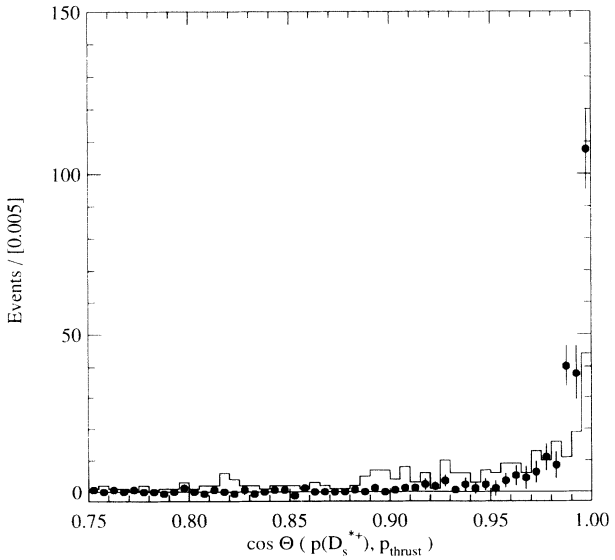

FIG. 8. The cosine of the angle between the D_s^{*+} direction and the thrust axis for our D_s^{*+} signal simulation using D^{*0} and D^{*+} events (solid points) and $b\to u\mu^-\bar\nu_\mu$ Monte Carlo data (histogram).

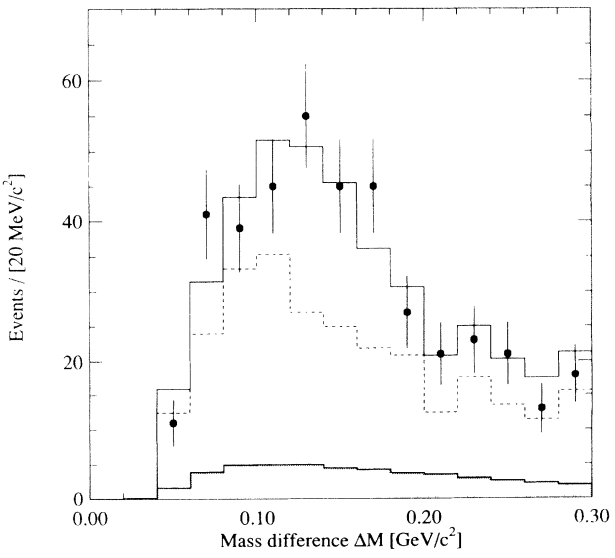

FIG. 9. The mass difference distribution for D_s^{*+} candidates, for both the muon data (solid points), the electron data (dashed histogram), and excess muon fakes over electron fakes (shaded). The histogram is the result of the likelihood fit described in the text.

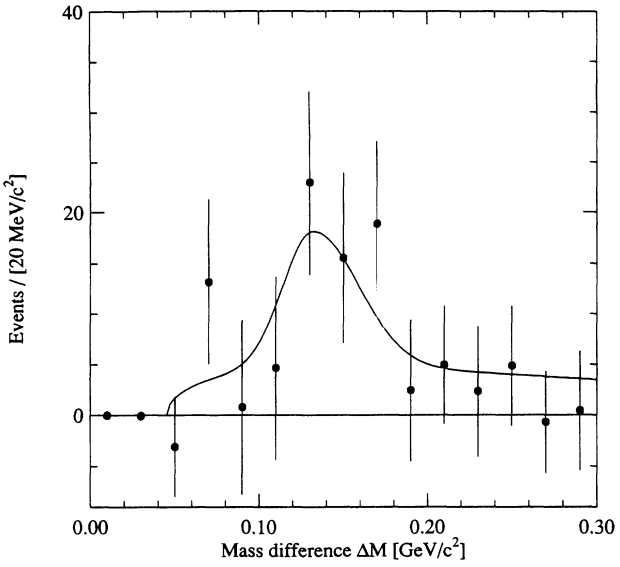

FIG. 10. The mass difference distribution for D_s^{*+} candidates with electrons and excess muon fakes subtracted. The curve is a fit to the signal shape described in the text.

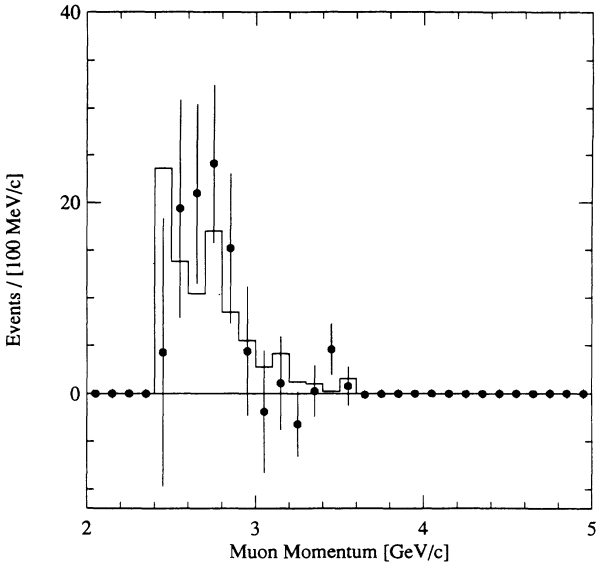

FIG. 12. The resulting muon momentum spectrum after electron and fake subtraction (solid points) compared with the prediction constructed from the proper sum of the D^{*0} and D^{*+} samples removing the π^+ (histogram).

the sum of three contributions: the scaled electrons, the excess of muon over electron fakes, and the signal distribution evaluated from the D^{*0} and D^{*+} samples discussed above (Fig. 7). Here the size of the electron and fake contributions are fixed and only the signal normalization is allowed to vary. We find 39±8 events in the peak which are attributed to the process $D_s^{*+} \to \gamma D_s^+$, $D_s^+ \to \mu^+ \nu$, and 54±11 events in the flat part of the distribution corresponding to the sum of $D_s^+ \to \mu^+ \nu$ and $D^+ \to \mu^+ \nu$ events coupled with a random photon [4].

To explicitly display the signal, we show in Fig. 10 the ΔM distribution after the electron and the fake subtraction. The histogram is a fit of the data to the signal shape calculated from the D^{*0} and D^{*+} samples. The χ^2 of the fit is 6 for 12 degrees of freedom. We find a total of 38±10 events which result from $D_s^{*+} \to \gamma D_s^+$, $D_s^+ \to \mu^+ \nu$ in the mass peak centered near the known $D_s^{*+} - D_s^+$ mass difference, with the remaining 52±14 events being

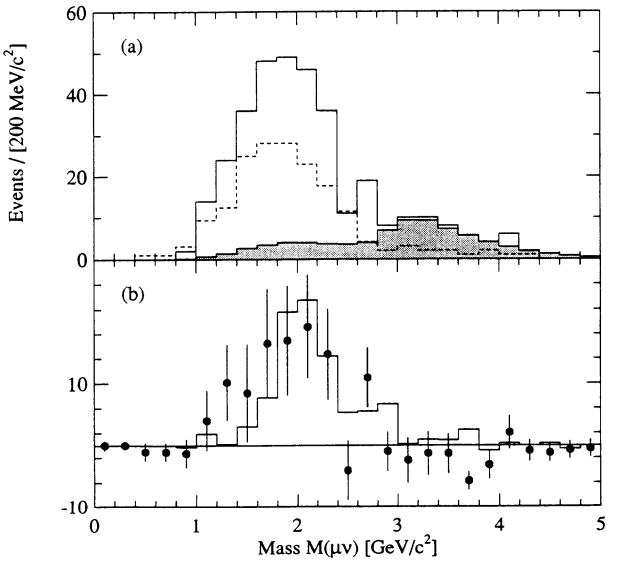

FIG. 11. The $M(\mu\nu)$ mass distribution (a) for D_s^{*+} candidates, for both the muon data (solid histogram), the electron data (dashed histogram) and excess muon fakes over electron fakes (shaded). (b) shows the background subtracted data (solid points). The histogram is the fit to the D^{*0} and D^{*+} data.

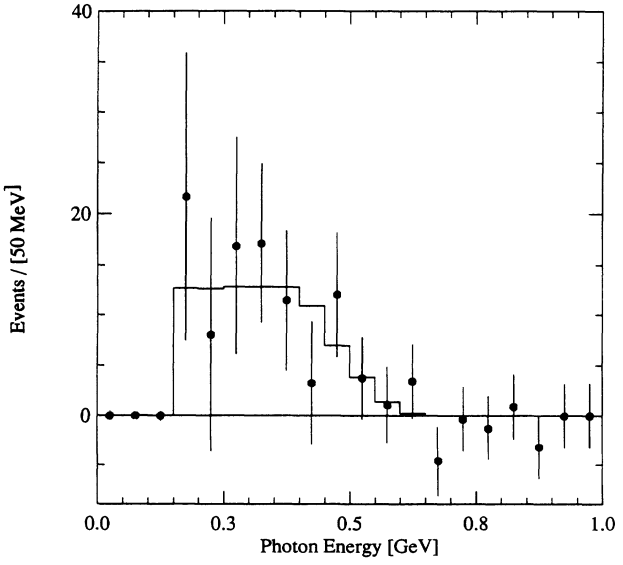

FIG. 13. The resulting photon energy spectrum after electron and fake subtraction (solid points) compared with the $D_s^{*+} \to \gamma D_s^+$, $D_s^+ \to \mu^+ \nu$ Monte Carlo prediction (histogram).

TABLE I. Systematic errors on width ratio.

Source of error	Value	Size of error (%)
Muon fake rate	(0.61±0.14)%	19
Electron fake rate	(0.30±0.07)%	9
μ/e normalization	1.04±0.05	11
Detection efficiency	(2.5±0.4)%	13
D_s^{*+}/D_s^+ production ratio [4]	1.03±0.2	11
$\phi\pi^+$ normalization	6778±500±407	6
Total systematic error		30

attributed to $D_s^+ \to \mu^+\nu$ or $D^+ \to \mu^+\nu$ accompanied by a random photon [4]. The results are consistent with the ones found using the simultaneous likelihood fit.

To convince ourselves that the excess in the peak region is due to $D_s^+ \to \mu^+\nu$ we also look at the $M(\mu\nu)$ invariant mass (D_s^+ mass) distribution where the $D_s^{*+} - D_s^+$ mass difference satisfies $100 < \Delta M < 180$ MeV. Figure 11(a) shows the muon, the electron, and the fake difference data, while Fig. 11(b) shows the background subtracted muon distribution (data points) and a fit with the signal shape from the D^{*+} and D^{*0} data samples. There is a clear excess which has the right shape for $D_s^+ \to \mu^+\nu$. In Fig. 12, we plot the muon momentum spectrum after electron and fake subtraction, and in Fig. 13 we show the photon energy spectrum after electron and fake subtraction. These distributions agree with the expectations for $D_s^+ \to \mu^+\nu$.

Using the likelihood fit, we extract a width for $D_s^+ \to \mu^+\nu$ by normalizing to the fully reconstructed $D_s^{*+} \to \gamma D_s^+$, $D_s^+ \to \phi\pi^+$ decays found in Fig. 6(b). The efficiency for reconstructing the $\phi\pi^+$ decay is obtained from Monte Carlo data. We find

$$\frac{\Gamma(D_s^+ \to \mu^+\nu)}{\Gamma(D_s^+ \to \phi\pi^+)} = 0.245 \pm 0.052 \pm 0.074 , \quad (8)$$

where the first error is statistical and the second is systematic. The denominator is determined from the efficiency corrected number of D_s^{*+} events, 6778±500±407, which decay into $\gamma\phi\pi^+$ for D_s^{*+} momenta above 2.4 GeV/c. The statistical error includes the errors on the measured numbers of $\mu^+\nu$ and $\phi\pi^+$ events.

The systematic errors are given in Table I. The errors that arise from the relative muon/electron ratio normalization, the muon fake rate, the electron fake rate, and the D_s^{*+}/D_s^+ production ratio [4], are estimated by fitting the data with each parameter changed by $\pm 1\sigma$. The systematic error due to the detection efficiency is dominated by the statistics of our D^{*0} sample. We also include a systematic error of ±6% for the detection efficiency of the normalization mode $\phi\pi^+$ relative to $\mu^+\nu$.

VI. CONCLUSIONS

We have made the first measurement of the ratio of decay widths $\Gamma(D_s^+ \to \mu^+\nu)/\Gamma(D_s^+ \to \phi\pi^+)$. In order to extract the decay constant f_{D_s} the width for the $D_s^+ \to \phi\pi^+$ decay is required. The total D_s^+ width is well known because of precise lifetime measurements [2], but the absolute $\phi\pi^+$ branching ratio is not well established. Using theoretical models to relate the measured branching fractions $\mathcal{B}(D^+ \to \bar{K}^{*0} l^+\nu)$ and $\mathcal{B}(D_s^+ \to \phi l^+\nu)$ and the measured ratio of $\Gamma(D_s^+ \to \phi l^+\nu)/\Gamma(D_s^+ \to \phi\pi^+)$ an estimate for $\mathcal{B}(D_s^+ \to \phi\pi^+)$ of (3.7±0.9)% has been derived (see the Appendix). Using this result we find

$$f_{D_s} = 344 \pm 37 \pm 52 \pm 42 \text{ MeV} . \quad (9)$$

The first two errors are the statistical and systematics errors resulting from our relative branching ratio measurement, and the third error reflects the uncertainty in the absolute $D_s^+ \to \phi\pi^+$ branching ratio. There has recently appeared a report of six events which have been ascribed to $D_s^+ \to \mu^+\nu$ decay [13]. A value of $f_{D_s} = (232 \pm 45 \pm 20 \pm 48)$ MeV has been obtained from these events using an estimate of the D_s^+ production cross section derived by extrapolation from an experiment at a different center-of-mass energy. This value of f_{D_s} is lower than ours, but consistent, given the uncertainties in the $D_s^+ \to \phi\pi^+$ branching ratio and in the D_s^+ cross section.

Theoretical predictions of f_{D_s} have been made using many methods. Recent lattice gauge calculations [14] give 230 MeV, while potential model [15] values range from 210 to 356 MeV. QCD sum-rule estimates [16] are between 200 and 290 MeV. Predictions for f_{D_s} have also been made combining theory with experimental input. Using the assumption of factorization for $B \to D^* D_s^-$ decays combined with measured branching ratios, values of f_{D_s} range from 237 to 271 MeV with an error of about 50 MeV, when scaled to $\mathcal{B}(D_s^+ \to \phi\pi^+) = (3.7 \pm 0.9)\%$ [17]. Use of experimental data on isospin mass splittings in the D^* and D system gives a value for f_D of 290 MeV [18] (f_{D_s} is thought to be 10–20 % higher than f_D). Most of these theoretical predictions are lower than our value of f_{D_s}.

ACKNOWLEDGMENTS

We gratefully acknowledge the effort of the CESR staff in providing us with excellent luminosity and running conditions. J.P.A. and P.S.D. thank the PYI program of the NSF, I.P.J.S. thanks the YI program of the NSF, G.E. thanks the Heisenberg Foundation, K.K.G. and A.J.W. thank the TNRLC, K.K.G., H.N.N., J.D.R., and H. Y. thank the OJI program of DOE, and P.R. thanks the A.P. Sloan Foundation for support. This work was supported by the National Science Foundation and the U.S. Department of Energy.

APPENDIX

The absolute branching ratio for $D_s^+ \to \phi\pi^+$ can be estimated by measuring the decay width relative to the $\phi l^+\nu$ mode. The branching fraction $\mathcal{B}(D_s^+ \to \phi l^+\nu)$ can

TABLE II. Experimental data.

Experiment	$\Gamma(D_s^+ \to \phi l^+\nu)/\Gamma(D_s^+ \to \phi\pi^+)$
CLEO [20]	$0.49\pm0.10^{+0.10}_{-0.14}$
ARGUS [21]	$0.57\pm0.15\pm0.15$
E687 [24][a]	$0.58\pm0.11\pm0.08$
Average	0.55 ± 0.09
	R^{*+}
E691 [22]	$0.49\pm0.04\pm0.05$
E653 [23][a]	$0.46\pm0.07\pm0.08$
E687 [24][a]	$0.56\pm0.04\pm0.06$
CLEO [25]	$0.73\pm0.08\pm0.09$
Average	0.55 ± 0.04
	$\mathcal{B}(D^+ \to K^-\pi^+\pi^+)$ (%)
Mark III [26]	$9.1\pm1.3\pm0.4$
CLEO [27]	$10.0\pm1.0\pm1.2$
Average	9.5 ± 1.0

[a]These semimuonic width measurements are scaled up by 1.04 before averaging to correspond to the semielectronic width.

be related to the branching fraction $\mathcal{B}(D^+ \to \bar{K}^{*0} l^+\nu)$ by

$$\mathcal{B}(D_s^+ \to \phi l^+\nu) = \mathcal{F}\mathcal{B}(D^+ \to \bar{K}^{*0} l^+\nu)\frac{\tau_{D_s^+}}{\tau_{D^+}}, \qquad \text{(A1)}$$

where $\tau_{D_s^+}$ and τ_{D^+} are the D_s^+ and D^+ lifetimes, and $\mathcal{F}$ is a theoretical correction to account for differences in the $D^+ \to \bar{K}^{*0} l^+\nu$ and $D_s^+ \to \phi l^+\nu$ widths, which are nominally equal. Two models give different predictions for $\mathcal{F}$. Scora predicts $\mathcal{F}=1.02$, whereas a value of 0.83 is given by Wirbel *et al.* [19]. We average the two values and assign an error of ± 0.1.

Using CLEO [20], ARGUS [21], and the new E687 [24] measurements (see Table II) of the decay $D_s^+ \to \phi l^+\nu$ we get an average result of $\Gamma(D_s^+ \to \phi l^+\nu)/\Gamma(D_s^+ \to \phi\pi^+) = 0.55\pm0.09$.

The ratio of the decay widths

$$R^{*+} = \Gamma(D^+ \to \bar{K}^{*0} l^+\nu)/\Gamma(D^+ \to K^-\pi^+\pi^+)$$

has been measured by E691 [22] and E653 [23] (see Table II). Including new E687 [24] and CLEO [25] measurements we get an average value of $R^{*+} = 0.55\pm0.04$. For the absolute branching ratio of the decay $D^+ \to K^-\pi^+\pi^+$ we take the average of the Mark III [26] and the new CLEO [27] values, $(9.5\pm1.0)\%$.

Using the well-measured ratio of the lifetimes $\tau_{D_s^+}/\tau_{D^+} = 0.42\pm0.03$ we arrive at

$$\mathcal{B}(D_s^+ \to \phi\pi^+) = (3.7\pm0.9)\% \,. \qquad \text{(A2)}$$

[1] J. L. Rosner, in *Particles and Fields 3,* Proceedings of the 1988 Banff Summer Institute, Banff, Alberta, Canada, edited by A. N. Kamal and F. C. Khanna (World Scientific, Singapore, 1989), p. 395.

[2] Particle Data Group, K. Hikasa *et al.*, Phys. Rev. D **45**, S1 (1992).

[3] F. J. Gilman and M. B. Wise, Phys. Rev. D **27**, 1128 (1983).

[4] CLEO Collaboration, F. Butler *et al.*, Phys. Rev. Lett. **69**, 2041 (1992). The contribution of combinations of random photons with a real $D^+ \to \mu^+\nu$ decay is larger since the $D^{*+} \to \gamma D^+$ branching ratio does not enter in. It is estimated to be about (18±8)% relative to the total $D_s^+ \to \mu^+\nu$ plus random photon contribution and included in the analysis.

[5] CLEO Collaboration, Y. Kubota *et al.*, Nucl. Instrum. Methods A **320**, 66 (1992); the crystal performance is described in R. Morrison *et al.*, Phys. Rev. Lett. **67**, 1696 (1991).

[6] We calculate a likelihood, $\mathcal{L}$ based on the measured σ's. Then for a positive kaon interpretation we require $\mathcal{L}_K/(\mathcal{L}_\pi+\mathcal{L}_K+\mathcal{L}_p) > 0.75$, and similarly for protons.

[7] The thrust axis is moved away from the lepton momentum by an angle $\delta\theta = 230 - 35p_l$ mrad, where p_l is the lepton momentum in GeV/c.

[8] We find a factor of 2 improvement in efficiency and a factor of 2 increase in background using only one hemisphere to determine the missing momentum relative to using the whole event.

[9] CLEO Collaboration, D. Bortoletto *et al.*, Phys. Rev. Lett. **69**, 2046 (1992).

[10] CLEO Collaboration, J. P. Alexander *et al.*, Phys. Lett. B **303**, 377 (1993); CLEO Collaboration, D. Bortoletto *et al.*, Phys. Rev. D **37**, 1719 (1988); it is assumed that the fragmentation functions for D^{*0} and D^{*+} are identical.

[11] D. Atwood and W. Marciano, Phys. Rev. D **41**, 1736 (1990).

[12] In the momentum range of interest, the probability for a pion to fake a muon is $(0.57\pm0.10)\%$, and the probability for a kaon to fake a muon is $(0.99\pm0.26)\%$. The probability for a proton or antiproton to fake a muon is negligibly small. The probabilities for pions or kaons or protons to fake electrons are averaged and are roughly constant in our momentum interval.

[13] S. Aoki *et al.*, Prog. Theor. Phys. **89**, 131 (1993).

[14] C. Bernard, J. Labrenz, and A. Soni, Phys. Rev. D **49**, 2536 (1994); C. Bernard *et al.*, *ibid.* **38**, 3540 (1988); G. Martinelli *Heavy Flavour on the Lattice: Results and Prospects,* Proceedings of the 5th International Symposium on Heavy Flavor Physics, Montreal, 1993 (Editions Frontières, Gif-sur-Yvette, in press); M. B. Gavela *et al.*, Phys. Lett. B **206**, 113 (1988); T. A. DeGrand and R. D. Loft, Phys. Rev. D **38**, 954 (1988).

[15] H. Krasemann, Phys. Lett. **96B**, 397 (1980); M. Suzuki, *ibid.* **162B**, 391 (1985); S. Godfrey and N. Isgur, Phys. Rev. D **32**, 189 (1985); S. N. Sinha, Phys. Lett. B **178**, 110 (1986); P. Cea *et al.*, *ibid.* **206**, 691 (1988); S. Capstick and S. Godfrey, Phys. Rev. D **41**, 2856 (1988).

[16] C. Dominguez and N. Paver, Phys. Lett. B **197**, 423 (1987); S. Narison, *ibid.* **198**, 104 (1987); L. J. Reinders, Phys. Rev. D **38**, 947 (1988); M. A. Shifman, Usp. Fiz. Nauk **151**, 193 (1987) [Sov. Phys. Usp. **30**, 91 (1987)].

[17] D. Bortoletto and S. Stone, Phys. Rev. Lett. **65**, 2951 (1990); J. L. Rosner, Phys. Rev. D **42**, 3732 (1990); ARGUS Collaboration, H. Albrecht *et al.*, Z. Phys. C **54**, 1 (1992).

[18] J. F. Amundson *et al.*, Phys. Rev. D **47**, 3059 (1993).

[19] D. Scora, in *Particles and Nuclei,* Proceedings of the Twelfth International Conference, Cambridge, Massachusetts, 1990, edited by J. L. Matthews *et al.* [Nucl. Phys. **A527** (1991)]; M. Wirbel *et al.*, Z. Phys. C **29**, 269 (1985).

[20] CLEO Collaboration, J. Alexander *et al.*, Phys. Rev. Lett. **65**, 1531 (1990).

[21] ARGUS Collaboration, H. Albrecht *et al.*, Phys. Lett. B **255**, 634 (1991).

[22] E691 Collaboration, J. C. Anjos *et al.*, Phys. Rev. Lett. **62**, 722 (1989).

[23] E653 Collaboration, K. Kodama *et al.*, Phys. Lett. B **286**, 187 (1992).

[24] E687 Collaboration, P. Sheldon, Proceedings of the 5th International Symposium on Heavy Flavor Physics (Ref. [14]).

[25] CLEO Collaboration, A. Bean *et al.*, Phys. Lett. B **317**, 647 (1993).

[26] Mark III Collaboration, J. Adler *et al.*, Phys. Rev. Lett. **60**, 89 (1988).

[27] CLEO Collaboration, R. Balest *et al.*, Phys. Rev. Lett. **72**, 2328 (1994).

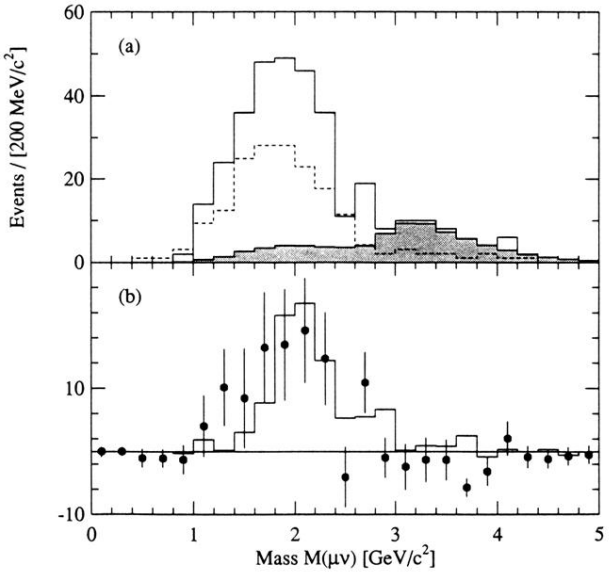

FIG. 11. The $M(\mu\nu)$ mass distribution (a) for D_s^{*+} candidates, for both the muon data (solid histogram), the electron data (dashed histogram) and excess muon fakes over electron fakes (shaded). (b) shows the background subtracted data (solid points). The histogram is the fit to the D^{*0} and D^{*+} data.

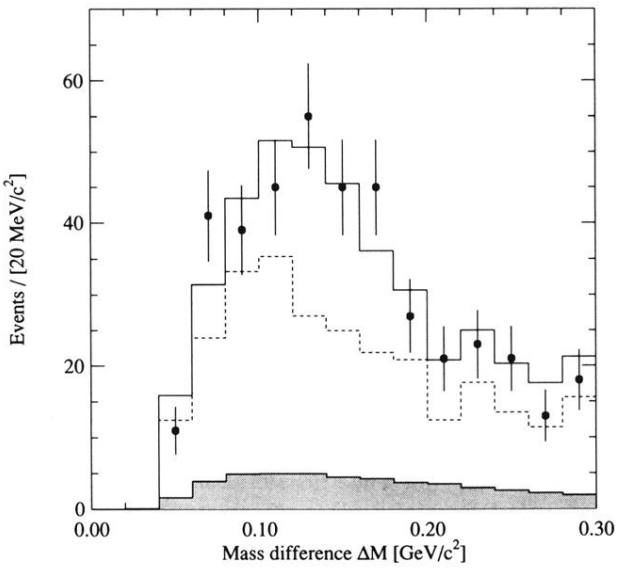

FIG. 9. The mass difference distribution for D_s^{*+} candidates, for both the muon data (solid points), the electron data (dashed histogram), and excess muon fakes over electron fakes (shaded). The histogram is the result of the likelihood fit described in the text.